



Spectroscopic and Theoretical Explorations on 6-Hydromethyl-4-Methoxy-4- Methoxytetrahydro- Pyran-2, 3, 5-Triol-A Biomolecule

M. Krishna Priya¹, S. Krithika¹, D. Angeline Shirmila¹, S. Sathya² and G. Usha^{1*}

¹Department of Physics, Queen Mary's College, Affiliated to the University of Madras, Chennai-04, India.

²Department of Physics, Bakthavatchalam College, Affiliated to University of Madras, Chennai-80, India.

Authors' contributions

This work was carried out in collaboration among all authors. Author MKP choose the research problem, performed the experiment, data collection and the analysis, wrote the manuscript. Author SK managed the extraction of the compound. Authors DAS and SS contribute to the analyses of the study. Author MKP managed the whole manuscript and checked for its correctness and validate the results. All authors read and approved the final manuscript.

Article Information

DOI: 10.9734/AJOCS/2021/v9i219067

Editor(s):

(1) Prof. Pradip K. Bhowmik, University of Nevada Las Vegas, Las Vegas.

Reviewers:

(1) Dr. Aslihan Yilmaz Obali, Selcuk University, Turkey.

(2) Apt. Galih Satrio Putra, University of Anwar Medika Hospital, Indonesia.

Complete Peer review History: <http://www.sdiarticle4.com/review-history/64557>

Original Research Article

Received 10 November 2020

Accepted 16 January 2021

Published 09 February 2021

ABSTRACT

The chemical compound 6-hydromethyl-4-methoxy-4- methoxytetrahydro-pyran-2, 3, 5-triol ($C_7H_{14}O_6$), was derived from the ethanol extract of *Senna auriculata* flower via GC-MS. FT-IR and NMR characterization of the compound support covalent bonding information and degree of degeneracy, respectively. 3D molecular structure was optimized to enhance the accuracy of computations. MEP, NBO, HOMO-LUMO, and Mulliken charge distribution studies provide details like reactive sites, electron density dislocation, and molecular interactions, charge transfer within the molecule and frontier orbital energies, electron density on the individual atom, and these were computed using hybrid B3-LYP quantum level with 6-311++G(d, p) basis set. Thermodynamic properties such as heat capacity, entropy, enthalpy, and their relation with temperature changes for the title molecule were also analyzed using THERMO.PL software. Non-linear optical properties

*Corresponding author: E-mail: guqmc@yahoo.com;

namely polarizability, first-order hyperpolarizability, and electronic dipole moment have also been computed at B3-LYP level with 6-311++G (d, p) basis set. Docking simulation was initiated on the title molecule using Autodock 4.2 software and found to be an excellent inhibitor of ALR2, an enzyme.

Keywords: GC-MS; DFT; HOMO-LUMO; NBO; IN-SILICO; docking.

1. INTRODUCTION

Natural or synthetic compounds containing heterocyclic pyran moiety are well known for their biological activities and play a vital role as lead a molecule in the field of drug designing. Pyran moiety is a core unit in benzopyrans, chromones, coumarins, flavonoids, and numerous naturally occurring compounds, and exhibits pharmacological activities such as anti-viral [1], antimicrobial [2], antitumor [3], cancer therapy [4], antifungal [5], antidiabetic [6], and anti-inflammatory [7,8]. The field of medicine is greatly influenced by chromenes due to their antivasular [9], anti-oxidant [10], antifungal [11], antiviral [12], antimalarial [13], antiproliferative [14], anti-Alzheimer, anti-Parkinson and Huntington's diseases [15,16], Coumarins (1-benzopyran-2-one) are naturally found in many plants possess a variety of biological properties, including antimicrobial, antiviral, anti-inflammatory, antidiabetic, antioxidant, and enzyme inhibitory activity. Flavonoids are rich sources of natural antioxidants in human diets and they neutralize the harmful effects of free radicals and thus aid in the prevention of many diseases. International Diabetes Federation predicts as many as 438 million will have diabetes by 2030 and the number of Americans with diabetes projected to be doubled or triple by 2050. Diabetes is a group of diseases that involve problems with the hormone insulin and occur when the pancreas produces very little or no insulin. As yet, there is no cure; diabetes causes an estimated death of 3.2-5.0 million per year. The pathogenic mechanism leading to diabetic complications is usually linked to increased activity of the enzyme Aldose Reductase (ALR2). Using Autodocking algorithms, an in-silico design to complement and accelerate in-vivo practices had been carried out to understand the capability of the title compound as an effective enzyme Aldose Reductase inhibitor (ALR2).

The worldwide prevalence of Covid-19 or Corona Virus and its implication (increased mortality) on diabetic patients have prompted us to take the present antidiabetic study on the title

molecule using DFT method and in-silico evaluation.

2. EXPERIMENTAL

2.1 6-Hydromethyl-4-Methoxy-4-Methoxytetrahydro-Pyran-2, 3, 5-Triol from GC-MS Result

The flowers of *Cassia auriculata* Linn were collected from Udumalpet, Tamil Nadu, dried under shade and crushed into a coarse powder. Then the powder was completely soaked in ethanol (solvent) and stirred well using a magnetic stirrer at constant temperature (780rpm) for about 2h, and filtered for the extract of the flowers of *Cassia auriculata*. The GC-MS spectra of the extract were obtained using the JEOL GCMATE II GC-MS with helium temperature 150°C, helium flow rate 2.8 L/min., chemical ion source, capillary type of column, and data system available in the sophisticated analytical instrumentation facility at IIT-M, Chennai. 6-hydromethyl-4-methoxy-4-methoxy tetrahydro-pyran-2, 3, 5-triol is one of the eight chemical compounds identified from the ethanol extract of the flowers of *Cassia auriculata* using GC-MS spectral data

2.2 Spectroscopic and Computational Particulars

The experimental Fourier transform infrared spectrum (FT-IR) of the *Cassia auriculata* flower extract was recorded in the range of 4000-400cm⁻¹, Model FT/IR-4100typeA at SAIF, Indian Institute of Technology (IIT-M), Chennai. Optimized 3D molecular structure and stabilization energy, normal mode frequencies and the associated wave number assignments based on potential energy distribution (PED), ¹H, ¹³C NMR spectra, reactive sites on molecular surface (MEP), charge transfer within the molecule (HOMO-LUMO), electron population over individual atoms (Mulliken charges), molecular interactions and thus the stability of the compound (NBO), and NLO properties of the title molecule was computed by

DFT-B3LYP level with 6-311++G(d, p) basis set using Gaussian 09W software program package [17]. The relationship between thermodynamical variables and the temperature was established using THERMO.PL [18].

3. RESULTS AND DISCUSSION

3.1 Optimized Molecular Geometry

The 3D molecular structure (Fig. 1) was obtained using the 2D chemical structure of the title molecule as input to Gaussian 09W and studied for its optimized geometries at B3LYP level with 6-311++G(d,p) basis set by GIAO approach [19]. The molecule, $C_7H_{14}O_6$, consisting of 27 atoms including a six-membered heterocyclic pyran ring, and those atoms were bonded via C-C, C-O, and C-H single bonds. In the structure, the C-C, C-O and C-H single bond distances (Table 1)

are in the range of 1.5539-1.5728Å, 1.4248-1.4365Å and 0.9609-1.101Å, respectively, and these values are in good agreement with the experimental values [20]. Negligibly small deviation observed between the experimental and theoretical bond geometries may be because the X-ray diffraction data were collected using a sample in the solid-state whereas theoretical computations were performed in the gaseous state of the material.

The various bond angles around C atom [C-C-O, O-C-H, C-C-C, H-C-H, H-C-O, O-C-H and O-C-C] are lies between $[104.0406-116.0061]^\circ$, representing the distorted tetrahedron structure of the molecule. The pyran ring of the title molecule adopts chair conformation (the shape assumed by the ring) which is shown in Fig. 2.

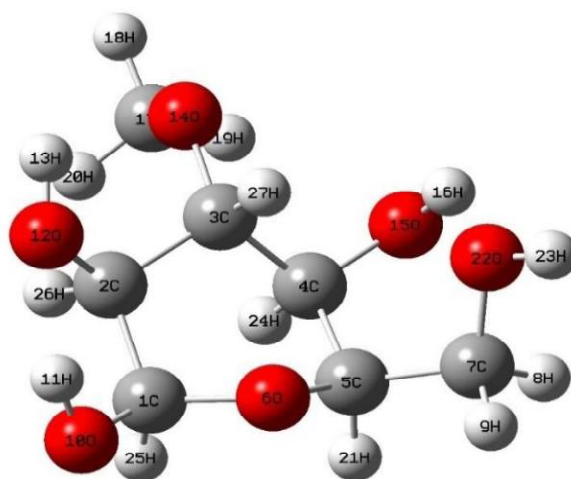


Fig. 1. Optimized 3D Molecular Structure

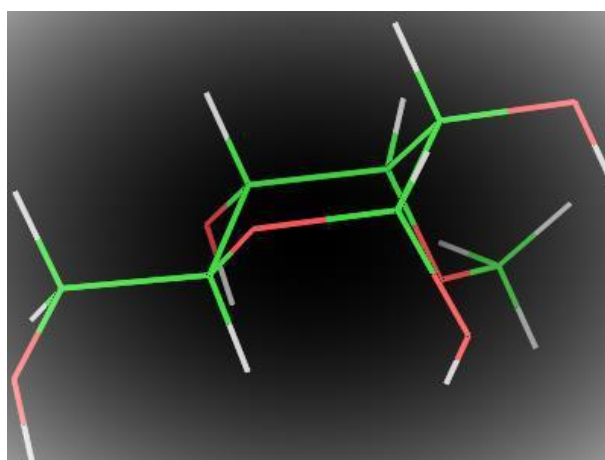


Fig. 2. Ring Conformation of the pyran ring

Table 1. Optimized bond geometries

Atoms	Distance (Å)/Angle(°)	Atoms	Angle (°)
C1–C2	1.5539	C2–C1–O6	109.4549
C1–O6	1.4298	C2–C1–O10	112.7043
C1 – O10	1.379	C2–C1–H25	109.8769
C1 – H25	1.0989	O6–C1–O10	109.3076
C2–C3	1.5337	O6–C1- H25	108.058
C2 – O12	1.4263	O10 – C1 – H25	107.3166
C2 – H26	1.0977	C1–C2–C3	110.2538
C3–C4	1.5385	C1– C2– O12	108.219
C3 – O14	1.4253	C3–C2– O12	110.4605
C3 – H27	1.0922	C3–C2– H26	110.3014
C4–C5	1.5728	O12 – C2 – H26	109.1229
C4 – O15	1.4161	C2–C3–C4	110.124
C4 – H24	1.094	C2–C3–O14	111.0077
C5–O6	1.4281	C4–C3–O14	116.0061
C5–C7	1.5212	C4–C3–H27	107.7989
C5 – H21	1.101	O14 – C3 – H27	104.0406
C7–H8	1.0948	C3–C4–C5	107.7947
C7–H9	1.0935	C3–C4–O15	113.3086
C7 – O22	1.4365	C5–C4–O15	113.3584
O10 – H11	0.9685	O15 – C4 – H24	104.3527
O12 – H13	0.9644	C4–C5–O6	111.7713
O14 – C17	1.4248	C4–C5–C7	113.3945
O15 – H16	0.9684	C4–C5–H21	108.6944
C17 – H18	1.0901	O6–C5–C7	107.0762
C17 – H19	1.0935	O6–C5–H21	108.8188
C17 – H20	1.0972	C7–C5–H21	106.8927
O22 – H23	0.9609	C1–O6–C5	112.5604
C4 – O15 – H16	107.5584	C5–C7 – H8	109.334
O14 – C17 – H18	105.9769	C5–C7–H9	107.8401
O14 – C17 – H19	111.1136	C5–C7–O22	109.5498
O14 – C17 – H20	112.4154	H8–C7–H9	109.2913
C1 – O10 – H11	107.4534	H8–C7–O22	109.9711
C2 – O12 – H13	108.0068	H9–C7- O22	110.8141

3.2 Normal Mode Frequencies Assignment- FT-IR

There are 27 atoms in the non-linear molecule 6-hydromethyl-4-methoxy-4-methoxy tetrahydropyran-2,3,5-triol, and thus the normal modes of vibrations of the molecule [3N-6] is 75 as listed in Table S1. FT-IR spectrum recorded experimentally following KBr pellet technique in the range 4000-450 cm^{-1} along with the theoretically obtained spectrum using the DFT method, the integrated B3LYP level with 6-311++G(d, p) basis set is depicted in Fig. 3. Potential Energy Distribution (PED) was estimated for all the 75 normal modes of vibration among the local coordinates and using the software program GAR2PED [21]. Normal mode frequencies and the associated wave numbers were assigned based on the information provided by PED calculations. The

mismatch observed between the experimental and theoretical vibrational frequencies (Table S1) is attributed to an incomplete basis set, unaccounted electron correlation, anharmonicity in vibrations and inaccurate estimation of force constants. The systematic errors introduced by the above-said shortcomings can be diminished by scaling procedure [22]. For B3LYP/6-311++G(d, p) level of calculations, the wave numbers above 1700 cm^{-1} are scaled as 0.958 and below 1700 cm^{-1} scaled as 0.983 [23], and this makes the theoretical values much closer to the experimental values.

The O-H, C-H, O-C and C-C (ring) stretching vibrations are generally expected to occur around the wave number 3500, 2900, 1300 and 900 cm^{-1} , respectively, in the FT-IR spectrum [24-28]. In this work, the broad absorbance band around 3400 cm^{-1} is assigned to O-H stretching

vibrations in the experimental spectrum while the peaks around 2900, 1100 and 800 cm^{-1} are ascribed to C-H, O-C and C-C(ring) stretching vibrations. However, the wave numbers in the range 3709-3588 (100%PED), 2993-2850(\approx 100% PED), 1103-832 cm^{-1} (O-C 47%PED and C-C ring 28%PED) are attributed to O-H, C-H, O-C and C-C(ring) normal mode vibrations in the theoretically recorded FT-IR spectrum. Normal mode vibration observed around 1400 cm^{-1} in the experimental FT-IR and in the range 1370-1353 cm^{-1} (75% PED) in theoretical spectra is accredited to HCO bending vibration.

3.3 NMR Spectral Analysis

The NMR spectrum of the title sample is not recorded experimentally but recorded theoretically using integrated DFT -B3LYP with 6-311++G(d, p) basis set available in Gaussian 09W software package. From the ^1H NMR spectrum (Fig. S1), it is clear that except 8H and 13H all other hydrogen atoms are occupying the same energy state ($n=1$) and thus the degree of degeneracy is 12. Hydrogen atoms 8H and 13H are associated with $n=2, 3$ energy states, respectively. Whereas the ^{13}C NMR spectrum (Fig. S1) shows the carbon nuclei occupying the same energy state ($n=1$). Theoretically computed resonance peak positions in ^1H NMR and ^{13}C NMR spectra and the chemical shift with respect to Tetramethylsilane (TMS) are listed in Table S2 and Table S3, respectively. Generally, deshielded/shielded nuclei resonate at higher/lower δ ppm values. The observed chemical shift (δ ppm) values from both ^1H NMR and ^{13}C NMR spectra are in good agreement with the literature and reported values [29].

3.4 Molecular Electrostatic Potential (MEP)

The molecular electrostatic potential energy values for the title molecule is calculated using B3LYP/6-311++G (d, p) basis set at the optimized geometry level and the MEP map of the title compound is shown in Fig.4. Electrostatic potential energy is basically a measure of the strength of the nearby charges, nuclei and electrons, at a particular position [30]. In order to make the electrostatic potential energy data easy to interpret, a color spectrum, with red as the lowest electrostatic potential energy value and blue as the highest [31,32], is applied to convey the varying intensities of the electrostatic potential energy values.

In the present analysis, MEP of the title molecule shows no strong potential regions for electrophilic and nucleophilic strike. Less intense blue color around H23 atom and yellowish orange color over the oxygen atoms O6, O10, and O12 represent the weak electrophilic and nucleophilic charge centers, respectively. Absence of electronegative atomic regions ruled out the possibility for the intra and intermolecular hydrogen bond formation and thus the van der Waals forces play a vital role in stabilizing the molecule.

3.5 Frontier Molecular Orbital Analysis

The molecular energies corresponding to the HOMO-LUMO molecular orbital and the energy gap between them have been calculated using TD-DFT at B3LYP level with 6-311++G (d, p) basis set for the title molecule. The energy gap between the HOMO-LUMO molecular orbital is the measure of the rate of charge transfer between the frontier molecular orbital and thus the electrical conductivity [33, 34]. The surface representing the HOMO orbitals covered the entire molecule whereas the surface that of LUMO orbital invade only the fraction of the molecular surface (Fig. 5). This difference actually demonstrates the readiness of HOMO orbital to donate electrons and LUMO orbital to accept electrons, and also explains the σ - σ^* type excitation across the molecular orbital. Moreover, the large differences in the charge distribution between the HOMO-LUMO orbitals pave way for the effective charge transfer across the energy gap or within the molecule. The frontier molecular orbital (FMO) analysis has been carried out to deduce knowledge about the distribution of charge density within the molecule, regions of exchange of charge density, interaction between molecules, calculation of HOMO-LUMO energies and the energy gap, molecular reactivity, capacity of the molecule to absorb light and chemical reactivity of the molecule [35-38]. For the title molecule the calculated HOMO-LUMO energies are -7.054592 eV and -0.594360 eV, respectively, and the estimated HOMO-LUMO energy gap is 6.46023 eV. Generally, HOMO energy is the estimated value of ionization potential (energy required to dislodge the electron from HOMO) while that of LUMO is the electron affinity (the neutral atom's likelihood of gaining an electron). FMO analysis can also be used to compute global chemical reactivity descriptors namely Electronegativity (χ), chemical potential (μ), global hardness (η), softness (S), and electrophilicity index (ψ). These

global reactivity descriptors for the title molecule were computed theoretically and are listed in Table 2. The high IP and very low EA values support the greater strength and stability of the present compound. Rigidity of the

molecule is confirmed from the larger hardness and smaller softness values. The chemical descriptor electrophilicity index (ψ) assists in explaining the biological activity of the title molecule [39].

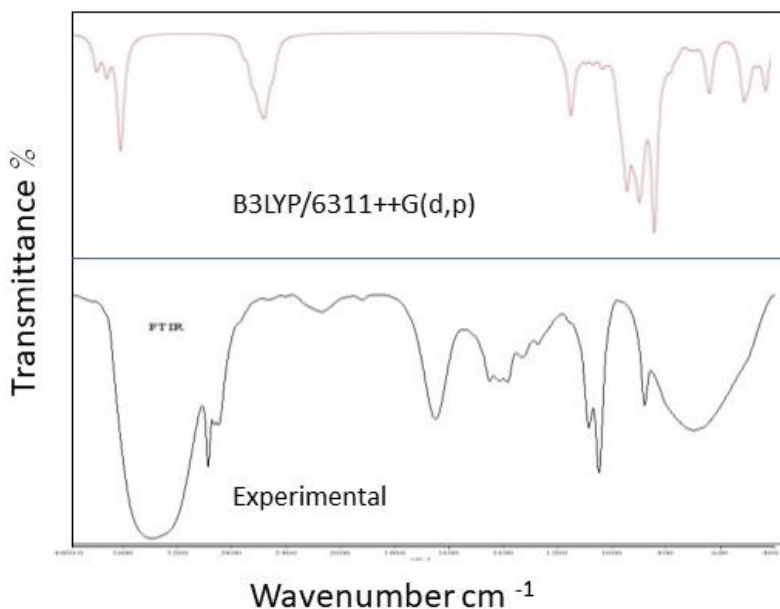
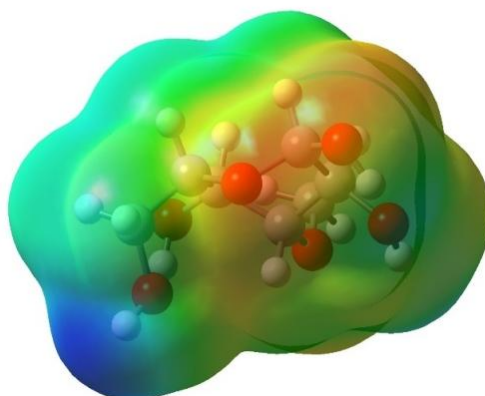


Fig. 3. Experimental and theoretical FTIR spectra of the title molecule



red < orange < yellow < green < cyan < blue

Fig. 4. Molecular Electrostatic Potential energy surface of the title molecule

Table 2. Theoretically computed values of the global chemical reactivity descriptors

Chemical descriptors	Computed values	Chemical descriptors	Computed values
E_{HOMO} (eV)	-7.054592	Chemical potential(μ)	-3.824476
E_{LUMO} (eV)	-0.59436	Electronegativity (χ)	3.824476
Energy gap (ΔE eV)	6.46023	Global hardness (η)	3.230116
Ionization potential(IP)	7.05492	Chemical softness(S)	0.309586
Electron affinity(EA)	0.59436	Electrophilicity (ψ)	2.264101

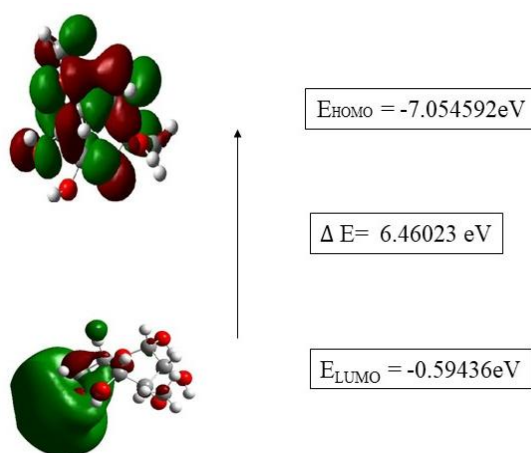


Fig. 5. The energy and the distribution of HOMO and LUMO orbitals

3.6 Estimation of Mulliken Charges

The Mulliken atomic charges are considered as the measure of electron density of each chemical species in the molecule [40] and they decide the molecular properties such as dipole moment, molecular polarizability, electronic structure, the magnitude of charge distribution over the chemical elements, interactions between the positively and negatively charged atoms and hydrogen bond formation, etc. [41,42]. For the title molecule, the Mulliken charges are estimated theoretically via the calculation of electron population of each atom using B3LYP level with 6-311++G (d, p) basis set and are listed in Table S4. The structural representation of the quantum of atomic charges is shown in Fig. 6. The charge distribution of the title molecule shows all the hydrogen atoms are positively charged. Except for the C5 carbon atom, all other carbon atoms along with oxygen atoms are with negative charges. The positive charges on the C5 carbon atom may be due to heavy negatively charged nearby oxygen atom O6. It is evident from the table that the atom C3 is distributed with maximum negative charges (-0.349781) while the atom H27 is with maximum positive charges (0.352040). The presence of large negative charges on carbon and oxygen atoms and net positive charges on hydrogen atoms advocate the formation of intermolecular interactions and consequently promote the formation of hydrogen bonds.

3.7 Natural Bonding Orbital (NBO) Analysis

NBO analysis is a well-chosen technique for the description of hyper conjugative interactions and

electron density transfer across the valence space. In hydrogen-bonded (X–H...Y) systems, the momentousness of hyper conjugative interactions and electron density transfer from filled lone electron pairs LP(Y) into an empty antibond σ^* (X–H) have been reported earlier [43-45].

The second-order Fock matrix was performed to elucidate the donor-acceptor interactions in NBO analysis at B3LYP level with 6-311++G (d, p) basis set [46] and those interactions always results in the loss of occupancy from the localized NBO of the idealized Lewis structure into an empty non-Lewis orbital. For each donor (i) and acceptor (j), the stabilization energy $E(2)$ associated with the delocalization $i \rightarrow j$ is estimated as $E(2) = \Delta E_{ij} = q_i (F_{ij})^2 \epsilon_j - \epsilon_i$, where, q_i is the donor orbital occupancy, ϵ_j and ϵ_i are diagonal elements and F_{ij} is the off-diagonal NBO Fock matrix element. For the present study, the NBO analysis outcomes are listed in Table S5. The highly intense interaction between electron donors and electron acceptors can be identified from the larger $E(2)$ value. The molecular stabilizing donor- acceptor interactions are generally due to the delocalization of electron density between occupied Lewis type to non-Lewis type NBO orbitals. From Table S5, the hyper conjugative interaction between the donor type σ (C1-C2) and the acceptor type σ^* (C2-O12) shows the highest stabilization energy 13.59kJ/mol followed by σ (C1-C2, C5-C4) with σ^* (C3-O4, C4-C5 and C1-C2) interaction energies 9.53, 9.06 and 6.89kJ/mol. In the present study the observed bonding- antibonding orbital interactions ($\sigma - \sigma^*$) show no significant contribution to the stabilization of the molecule.

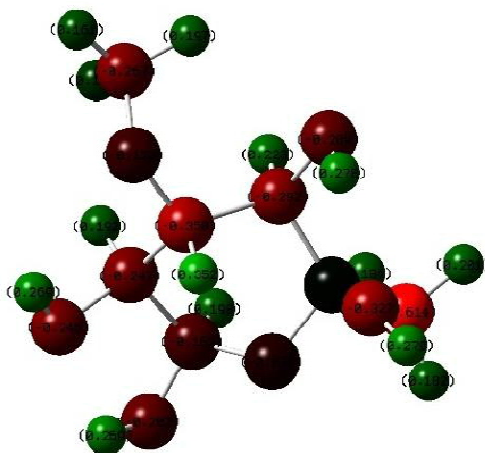


Fig. 6. Mulliken charges on individual atoms of the title molecule

3.8 Thermodynamic Parameters

The knowledge of vibrational frequencies computed based on the optimized geometrical parameters along with statistical thermodynamics are employed to estimate few a thermodynamic functions namely heat capacity ($C_{p,m}$), entropy (S_m), enthalpy (ΔH), and Gibbs free energy (ΔG). These thermodynamic parameters of the title molecule were estimated by the DFT/B3LYP level with 6-311++G (d,p) basis set at 298.15K and 1.00 atmospheric pressure and listed in Table S6. In practice, the changes in the thermodynamic functions with temperature over a range of 100-1000K was computed and they are found to increases with the increase of temperature. The relationship between the thermodynamic parameters and the temperatures was established using quadratic formulae [47] and the Scale factors have been introduced to narrow down the deviations of the computed parameters from that of observed parameters [48]. A graph is plotted as thermodynamic parameters Vs. temperature (Fig.S2) and the observed interdependence may be attributed to the increased vibrational intensities of the molecule with temperature [49].

The spontaneity of the adsorption process and the direction of chemical reactions can be derived from the data ΔG and the entropy, and of enthalpy, respectively. As a whole, the computation and analysis of thermodynamic parameters are of great help to note the thermal stability of the substance which is vital in defining the chemical reactivity descriptors of the title molecule and its suitability in biological activity studies.

3.9 Non-Linear Optical Activity

In this study, the anisotropic polarizability and its components, first-order hyperpolarizability, and its components along with dipole moment have been computed using DFT method at B3LYP level with 6-311++G(d,p) basis set by finite field approach and the values are listed in the [Table S7]. Estimates of various defining parameters [Table S7] have been performed using different formulas [50] and the obtained values are analyzed to comprehend the NLO capability of the title molecule. Urea is commonly treated as reference NLO material because of its non-centrosymmetric crystal packing and intramolecular charge transfer (ICT) adeptness. It is noteworthy to mention here that the enormous ' β ' (3.51158×10^{-25} e.s.u) and β_{zzz} (152.77205) values may be due to p-electron cloud movement from donor to the acceptor and the delocalization of electron cloud in that direction. The large value of hyperpolarizability and intramolecular charge transfer (ICT) of the title molecule demonstrate its suitability for NLO applications

3.10 *In silico* Analysis

In this work, the interactions of the title molecule (ligand) with Human Aldose Reductase (target) were examined by molecular docking studies. The three-dimensional structure of the target protein was taken from Research Collaboratory for Structural Bioinformatics (RCSB) Protein Databank (<https://www.rcsb.org/>) and the energy minimized conformation was appropriated as starting conformation for our docking studies. Preparation of both protein and ligand structures was completed using AutoDock Tools 1.5.6 [51]

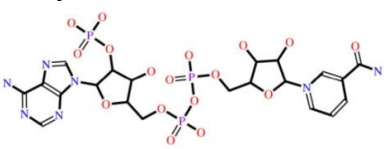
and molecular docking was performed using AutoDock 4.2.6 software [52]. Using the Auto Grid program, a Grid of size $40 \times 40 \times 40 \text{ \AA}^3$ with 0.375 \AA spacing was centered on co-crystallized ligand of the target. The Lamarckian Genetic Algorithm (LGA) [53] docking simulations were initiated with the number of requested GA docking of 10(runs) and maximum energy evaluation of 25×10^5 along with default values for other required parameters. At 298.15K, there are ten conformations and six active torsions about C-O and C-C bonds noted at the end of the docking procedure. Active site binding energy, inhibition constant, and intermolecular energy were perceived for each of the runs and are listed in Table 3. The intermolecular interactions between the ligand and the target established in the protein active site are listed in Table 4. Binding interaction between a small molecule (ligand) and an enzyme (target) may result in inhibition of the activity of that enzyme.

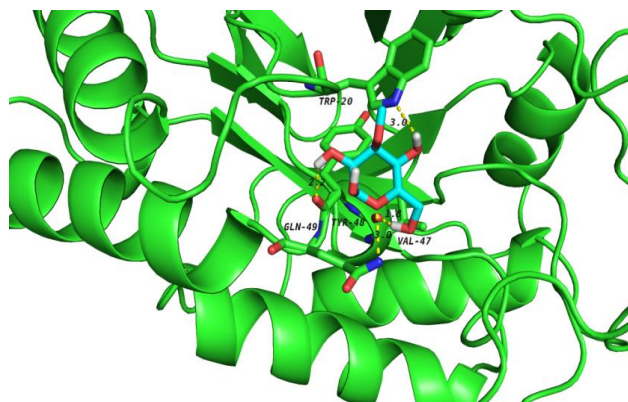
The binding mode interaction is characterized by a scoring function with minimum energy. Whereas the inhibition constant (K_i), the concentration needed to reduce the activity of that enzyme by half, is reflective of the binding affinity. The smaller the K_i , the greater the binding affinity and the smaller amount of medication needed to inhibit the activity of that enzyme. Based on the scoring function and other relevant parameters listed in Table 3, the docked pose corresponding to run 4 is considered as the best and the active site interactions [Fig.7] are listed in Table 4. The docking simulation of the title compound into the human ALR2 binding site offers a possible explanation for its good inhibitory activity and may guide the design of new analogues. Estimates of chemical reactivity descriptors and the results of MEP, NBO and HOMO-LUMO analysis also supported the outcome of molecular docking studies on the title molecule.

Table 3. Scoring functions obtained via molecular docking simulation

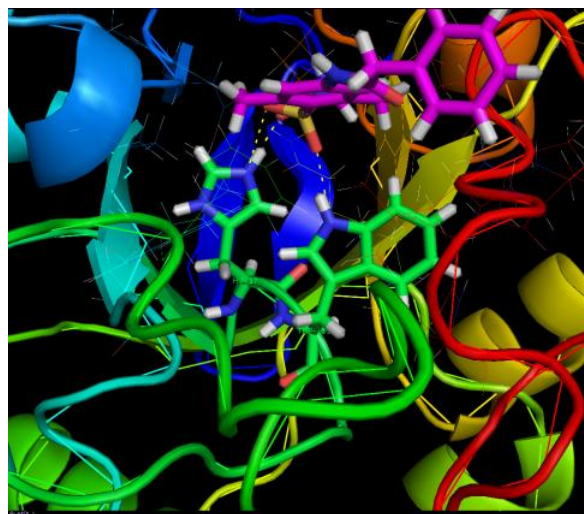
Run No.	Binding energy kcal/mol	Inhibition constant(K_i)mM	Intermolecular energy kcal/mol
1	-7.312	15.79	-4.25
2	-7.719	3.33	-5.17
3	-7.440	11.36	-4.44
4	-8.127	2.45	-5.35
5	-7.519	10.48	-4.49
6	-7.670	5.80	-4.84
7	-7.594	3.25	-5.08
8	-7.620	5.55	-4.87
9	-7.715	5.47	-4.88
10	-6.965	18.63	-4.15

Table 4. Binding site interactions and binding energies

Ligand	Run No./Pose	Binding site interaction	D-H...A (Å)	Binding energy kcal/mol
Co-crystal	5	HIS110(N-H...O) TRP111(N-H...O)	2.724 2.370	-6.714
	4	TRP20(O-H...O)	3.000	-8.127
		VAL47(O-H...O)	1.800	
		(N-H...O)TYR48	3.000	
		GLN49(O-H...O)	2.200	



[a]



[b]

Fig. 7. Pictures depicting interactions between ligand and target [a] Title molecule and [b] co-crystal

4. CONCLUSION

The pyran derivative has been recognized from the ethanol extract of *Senna auriculata* flower (Avaram Poo) using Gas Chromatography-Mass Spectrometry (GC-MS). All the computational work on the title molecule has been carried out using the DFT method at the B3LYP level with a 6311++G (D, P) basis set, incorporated in the Gaussian 09W software package. The 3D molecular structure was obtained and the bond geometries were estimated. The computed FTIR normal mode vibrations were assigned wave numbers based on PED (%) information and compared with experimentally recorded FTIR spectral frequencies. NMR spectrum of the title sample which aid in the estimates of the energy level of the individual atoms and the degree of

degeneracy of the molecule as a whole. Mapping of electrostatic potential gives assistance to visualize variably charged regions and the MEP of the title molecule shows no strong potential regions for the electrophilic and nucleophilic strike. The chemical reactivity descriptors derived from HOMO-LUMO analysis undeniably illustrate the intramolecular charge transfer and the appropriateness of the title molecule for biological activities. The characteristic electron population on distinct chemical species was estimated via Mulliken charges analysis. The molecular stabilizing due to the delocalization of electron density between NBO orbitals have been analyzed, which show no significant contribution to the stabilization of the molecule. The direct relationship between the thermodynamical variables such as heat

capacity, entropy, and enthalpy with temperature was also studied. The computed hyperpolarizability value supports the superiority of the title molecule over urea (standard) and thus this material can be best suited for optical applications. In-Silico investigation using Autodock algorithm available in Gaussian 09W platform disclose the active site interactions between the ligand (title molecule) and the target (enzyme - ALR2) and propose a possible explanation for its good anti-diabetic activity.

ACKNOWLEDGEMENT

Authors thank SAIF, IIT-Madras, Chennai-36 and DST-FIST, Queen Mary's College (A), Chennai-4 for providing instrumentation facilities.

COMPETING INTERESTS

Authors have declared that no competing interests exist.

REFERENCES

- Martínez-Grau A, Marco J. *Bioorg. Med. Chem. Lett.* 7;1997:3165–3170. DOI:https://doi.org/10.1016/S0960-894X(97)10165-2
- Khafagy MM, Abd El-Wahab AHF, Eid FA, El-Agrody AM. *Farmaco.* 2002;57:715–722 DOI:https://doi.org/10.1016/S0014-827X(02)01263-6
- Mohr SJ, Chirigos MA, Fuhrman FS, Pryor JW, *Cancer Res.* Pyran Copolymer as an Effective Adjuvant to Chemotherapy against a Murine Leukemia and Solid Tumor | *Cancer Research.* 1975;35:3750–3754. Available:aacrjournals.org
- Anderson DR, Hegde S, Reinhard E, Gomez L, Vernier WF, Lee L, Liu S, Sambandam A, Snider PA, Masih L, *Bioorg. Med. Chem. Lett.* 2005;15:1587–1590. DOI:https://doi.org/10.1016/j.bmcl.2005.01.067
- Radan Schiller, Lucie Tichotová, Jan Pavlík, Vladimír Buchta, Bohuslav Melichar, Ivan Votruba, Jiří Kuneš, Marcel Špulák, Milan Pour, *Bioorg. Med. Chem. Lett.* 2010; 20:7358–7360. DOI:https://doi.org/10.1016/j.bmcl.2010.10.052
- Bisht SS, Jaiswal N, Sharma A, Fatima S, Sharma R, Rahuja N, Srivastava AK, Bajpai V, Kumar B, Tripathi RP, *Carbohydr. Res.* 2011;346:1191–1201. DOI:https://doi.org/10.1016/j.carres.2011.03.006
- Wang SM, Milne GWA, Yan XJ, Posey IJ, Nicklaus MC, Graham L, Rice WGJ, *Med J. Chem.* 1996;39:2047–2054. DOI:https://doi.org/10.1021/jm950874+
- Wang Y, Mo SY, Wang SJ, Li S, Yang YC, Shi JG, *Org. Lett.* 7 (2005), 1675–1678. DOI:https://doi.org/10.1021/ol0475764
- Henriette Gourdeau, Lorraine Leblond, Bettina Hamelin, Clemence Desputeau, Kelly Dong, IrenejKianicka, Dominique Custeau, Chantal Boudreau, LilianneGeerts, Sui-Xiong Cai, John Drewe, Denis Labrecque, Shailaja Kasibhatla and Ben Tseng, *Mol. Cancer Ther.* 2004;3:1375-1384. Antivascular and antitumor evaluation of 2-amino-4-(3-bromo-4,5-dimethoxy-phenyl)-3-cyano-4H-chromenes, a novel series of anticancer agents | *Molecular Cancer Therapeutics* Available:aacrjournals.org
- Milan Mladenović, Mirjana Mihailović, DesankaBogojević, Sanja Matić, Neda Nićiforović, Vladimir Mihailović, NenadVuković, Slobodan Sukdolak&SlavicaSolujčić, *S. Int. J. Mol. Sci.* 2011;12(5):2822–2841. DOI:https://doi.org/10.3390/ijms12052822
- Thareja S, Verma A, Kalra A, Gosain S, Rewatkar PV, Kokil GR, *Acta. Pol. Pharm.* 2010; 67:423–427.423-427. qxd (ptfarm.pl)
- Paul W. Smith, Steven L. Sollis, Peter D. Howes, Peter C. Cherry, Ian D. Starkey, Kevin N. Copley, Helen Weston, Jan Scicinski, Andrew Merritt, Andrew Whittington, Paul Wyatt, Neil Taylor, Darren Green, Richard Bethell, Safia Madar, Robert J. Fenton, Peter J. Morley, Tony Pateman, Alan Beresford J. *Med. Chem.* 1998;41:787–797. DOI:https://doi.org/10.1021/jm970374b
- Andrade-Neto, VF de, Goulart, MOF, da Silva Filho, JF, da Silva MJ, Pinto MCF R, do, CFR, Pinto AV, Zalis MG, Carvalho LH, Krettli AU. *Bioorg. Med. Chem. Lett.* 2004; 14:1145-1149.
- Bianchi G, Tava A. *Agric. Biol. Chem.* 1987;51:200-2002.
- Andrani LL, Lapi E. *Boll. Chim. Farm.* 1960; 99:583–586.
- Zhang YL, Chen BZ, Zheng KQ, Xu ML, Lei XH, Yaoxue XB. *Chem. Abstr.* 1982; 96:135383e.

17. Frisch MJ, Trucks GW, Schlegel HB, Scuseria GE, Robb MA, Cheeseman JR, Scalmani G, Barone V, Mennucci B, Petersson GA, Nakatsuji H, Caricato M, Li X, Hratchian HP, Izmaylov AF, Bloino J, Zheng G, Sonnenberg JL, Hada M, Ehara M, Toyota K, Fukuda R, Hasegawa J, Ishida M, Nakajima T, Honda Y, Kitao O, Nakai H, Vreven T, JA Montgomery Jr., Peralta JE, Ogliaro F, Bearpark M, Heyd JJ, Brothers E, Kudin KN, Staroverov VN, Kobayashi R, Normand J, Raghavachari K, Rendell A, Burant JC, Iyengar SS, Tomasi J, Cossi M, Rega N, Millam JM, Klene M, Knox JE, Cross JB, Bakken V, Adamo C, Jaramillo J, Gomperts R, Stratmann RE, Yazyev O, Austin AJ, Cammi R, Pomelli C, Ochterski JW, Martin RL, Morokuma K, Zakrzewski VG, Voth GA, Salvador P, Dannenberg JJ, Dapprich S, Daniels AD, Farkas Ö, Foresman JB, Ortiz JV, Cioslowski J, Fox DJ. Gaussian, Inc., Wallingford CT;2009: 09.
18. Irikura KK, THERMO PL, National Institute of Standards and Technology; 2002.
19. Wolinski K, Haacke R, Hinton JF, Pulay P. Methods for parallel computation of SCR NMR Chemical shift by GIAO method: efficient integral calculation, multi-fockalgorithm and pseudodiagonalization, journal of computational chemistry. 1997; 18(6):c816-825.
DOI:[https://doi.org/10.1002/\(SICI\)1096-987X\(19970430\)18:6<816::AID-JCC7>3.0.CO;2-V](https://doi.org/10.1002/(SICI)1096-987X(19970430)18:6<816::AID-JCC7>3.0.CO;2-V)
20. Kovalskiy YP, Kinzhybalov VV, Karpiak NM et al. Chem Heterocycl Comp. 2011;46: 1443–1448.
DOI:<https://doi.org/10.1016/.molstruc.2018.02.22>
21. JML Martin, Van Alsenoy C, Gar2ped, University of Antwerp; 1995.
22. Yoshida H, Takeda K, Okamura J, Ehara A, Matsurra H, Phys J. Chem. A. 2002; 106:3580–3586.
DOI:<https://doi.org/10.1021/jp013084m>
23. Govindarajan M, Karabacak M, Periandy S, Tanuja D, Spectrochim. Acta A. 2012;97:231.
DOI:<https://doi.org/10.1016/j.saa.2012.06.014>
24. Sajjan D, Hubert Joe I, Jayakumar VS, Zaleski J, Mol J. Struct. 2006;785:43-53.
DOI:<https://doi.org/10.1016/j.molstruc.2005.09.041>
25. Socrates G, Infrared and Raman Characteristic Group Frequencies, third ed., Wiley Interscience Publications, New York; 1994.
26. Sun Y, Wang Y, Liu Z, Yu C, Spectrochim. Acta. 2012;96:42-50.
DOI:<https://doi.org/10.1016/j.saa.2012.04.094>
27. Surisseau C, Marvell P, Raman Spect J. 1994;25:447–455.
28. Barnes AJ, Majid MA, Stuckey MA, Gregory P, Stead CV, Spectrochim. Acta. 1985;A4:629–635.
29. Tintu K. Kuruvilla, Johanan Christian Prasana, Muthu S, Jacob George, Sheril Ann Mathew ,Spectrochimica Acta Part A: Molecular and Biomolecular Spectroscopy. 2018;188:382-393.
DOI:<https://doi.org/10.1016/j.saa.2017.07.029>
30. Murray JS, Sen K, Molecular Electrostatic Potentials: Concepts and Applications, Elsevier Science B.V., Amsterdam. 1996;182
31. Scrocco E, Tomasi J. Electronic molecular structure, Reactivity and intermolecular forces: An Euristic Interpretation by means of electrostatic molecular potential, Adv. Quantum chem. 1978;11115-193.
DOI:[https://doi.org/10.1016/S0065-3276\(08\)60236-1](https://doi.org/10.1016/S0065-3276(08)60236-1)
32. Fleming I, Frontier orbital and organic chemical reactions, Wiley, London,1976. N. Subramanian, N. Sundaraganesan, J. Jayabharathi, Spectrochim. Acta A. 2010; 76:259–269.
33. Curtiss LA, Redfern PC, Raghavachari K, Pople JA, aussian-3 theory using density functional geometries and zero-point energies, J. Chem. Phys. 1998;42:117-122.
34. Krishna Priya M, Revathi BK, Renuka V, Sathya S, Samuel Asirvatham P, Materials Today: Proceedings. 2019;8:37–46.
DOI:<https://doi.org/10.1016/j.matpr.2019.02.078>
35. Fleming I, Frontier Orbital and Organic Chemical Reactions, Wiley, London. 1976
36. Subramanian N, Sundaraganesan N, Jayabharathi J, Spectrochim. Acta A. 2010;76:259–269.
DOI:<https://doi.org/10.1016/j.saa.2010.03.033>
37. Socrates G, Infrared Characteristic Group Frequencies, Publications, Wiley Interscience. 1980
38. Varsanyi G. Vibrational Spectra of Benzene Derivatives, academic press, NewYork. 1969;31.

39. Chattaraj PM, Maiti B, Sarkar U, Am. Chem. Soc. 2003;107(25):4973–4975.
40. Mulliken RS, Chem J. Phys. 1955;23: 1831.
DOI:<https://doi.org/10.1063/1.1740588>
41. Kosar B, Albayrak C, Spectrochim. Spectrochim. Acta A. 2011;87:160-167.
DOI:<https://doi.org/10.1016/j.saa.2010.09.016>
42. Szafran, Komasa M, Adamska A, EBJ Mol. Struct. Theochem. 2007;827:101-107.
DOI:<https://doi.org/10.1016/j.molstruc.2006.05.012>
43. Weinhold F. Nature. 2001;411:539–541.
DOI:<https://doi.org/10.1038/35079225>
44. Weinhold F, Landis C. Valency and bonding: a natural bond orbital donor–acceptor perspective. Cambridge University Press, Cambridge; 2005.
45. Reed AE, Curtiss LA, Weinhold F, Chem. Rev. 1988;88:899–926.
DOI:<https://doi.org/10.1021/cr00088a005>
46. Leena Sinha, Mehmet Karabacak, Narayan, Mehmet Cinar V, Onkar Prasad, Spectrochim. Acta A. 2013;109:298-307.
47. Noureddine Issaoui, Houcine Ghalla, Muthub S, Flakus HT, Brahim Oujia. Spectrochimica acta part a: molecular and biomolecular spectroscopy. 2015;136: 1227–1242.
DOI:<https://doi.org/10.1016/j.saa.2014.10.008>
48. Varsanyi G, Sohar P, Acta Chim. Acad. Sci. Hung. 1972;74.
49. Bevan Ott J, Boerio-Goates J, Calculations from Statistical Thermodynamics, Academic Press; 2000.
50. Balamurugan N, Charanya C, Sampath Krishnan S, Muthu S. Spectrochimica acta part a: molecular and biomolecular spectroscopy. 2015;137:1374–1386.
DOI:<https://doi.org/10.1016/j.saa.2014.09.048>
51. Sanner MF. Python: A programming language for software integration and development. J. Mol. Graph. Model. 1999; 17:57–61.
52. Morris GM, Huey R, Lindstrom W, Sanner, MF, Belew RK, Goodsell DS, Olson AJ. Auto Dock 4 and Auto Dock Tools 4: Automated docking with selective receptor flexibility. J. Comput. Chem. 2009;30:2785–2791.
DOI:<https://doi.org/10.1002/jcc.21256>
53. Morris GM; Goodsell DS; Halliday RS; Huey R; Hart WE; Belew RK; Olson AJ. Automated docking using a Lamarckian genetic algorithm and an empirical binding free energy function. J. Comput. Chem. 1998;19:1639–1662.
DOI:[https://doi.org/10.1002/\(SICI\)1096-987X\(19981115\)19:14<1639::AID-JCC10>3.0.CO;2-B](https://doi.org/10.1002/(SICI)1096-987X(19981115)19:14<1639::AID-JCC10>3.0.CO;2-B)

© 2021 Priya et al.; This is an Open Access article distributed under the terms of the Creative Commons Attribution License (<http://creativecommons.org/licenses/by/4.0>), which permits unrestricted use, distribution, and reproduction in any medium, provided the original work is properly cited.

Peer-review history:
The peer review history for this paper can be accessed here:
<http://www.sdiarticle4.com/review-history/64557>